

# Flow-induced thermal effects on spatial DNA melting

Niel Crews,<sup>a</sup> Tim Ameen,<sup>a</sup> Carl Wittwer<sup>b</sup> and Bruce Gale<sup>\*a</sup>

Received 25th April 2008, Accepted 1st July 2008

First published as an Advance Article on the web 29th August 2008

DOI: 10.1039/b807034b

Continuous-flow temperature gradient microfluidics can be used to perform spatial DNA melting analysis. To accurately characterize the melting behavior of PCR amplicon across a spatial temperature gradient, the temperature distribution along the microfluidic channel must be both stable and known. Although temperature change created by micro-flows is often neglected, flow-induced effects can cause significant local variations in the temperature profile within the fluid and the closely surrounding substrate. In this study, microfluidic flow within a substrate with a quasi-linear temperature gradient has been examined experimentally and numerically. Serpentine geometries consisting of 10 mm long channel sections joined with 90° and/or 180° bends were studied. Infrared thermometry was used to characterize the surface temperature variations and a 3-D conjugate heat transfer model was used to predict interior temperatures for multiple device configurations. The thermal interaction between adjacent counter-flow channel sections, which is related to their spacing and substrate material properties, contributes significantly to the temperature profile within the microchannel and substrate. The volumetric flow rate and axial temperature gradient are directly proportional to the thermal variations within the device, while these flow-induced effects are largely independent of the cross-sectional area of the microchannel. The quantitative results and qualitative trends that are presented in this study are applicable to temperature gradient heating systems as well as other microfluidic thermal systems.

## Introduction

Microfluidic thermal devices can be used to induce temperature changes in small liquid volumes. Steady-state systems heat, cool, and thermally cycle by passing the fluid through microchannels within a substrate that contains a set temperature distribution. This technique is the mechanism behind continuous-flow PCR (CF-PCR), which uses a constant sample flow through a single channel to achieve the desired thermocycling. Microfluidic CF-PCR devices can be classified according to the substrate temperature field. The most common configuration consists of multiple isolated isothermal zones within the substrate with a long microfluidic channel transiting all zones. In devices of this type, the fluid mean velocity and microchannel length across each isothermal zone determine the sample residence time at each temperature. Heating elements typically contact the substrate above and/or below the zones, in parallel strips<sup>1</sup> or in quadrant divisions.<sup>2</sup> Substrate materials including glass,<sup>3,4</sup> glass-silicon,<sup>5</sup> glass-PDMS,<sup>6,7</sup> and polycarbonate (PC)<sup>8</sup> have been used.

In contrast to this multi-zone technique, a steady-state temperature gradient can be similarly used to control fluid temperature. Mao and co-workers<sup>9</sup> demonstrated this with an array of straight parallel microchannels under no-flow condi-

tions. By placing the array perpendicular to a spatially linear gradient such that each channel was positioned along a distinct isothermal line, the stationary fluid in each channel reached a uniform discrete temperature. By placing the array parallel to the gradient, a linear temperature gradient developed within the fluid of each channel, equal to the gradient in the substrate. Crews *et al.*<sup>10</sup> later expanded this work by introducing fluid flow and more advanced channel geometries. Temperature ramp rates for the fluid passing through the continuous-flow system were dictated by the local fluid mean velocity and flow direction relative to the isothermal lines of the temperature gradient. Thirty cycle and forty cycle devices were used to perform PCR from human genomic DNA template.<sup>11</sup> With a single cycle device, the spatial DNA melting analysis of multiple pre-amplified samples was achieved.<sup>12</sup> Temperature-induced melting of double-stranded DNA occurs within a narrow temperature range that is largely governed by its nucleotide composition and sequence.<sup>13</sup> In multi-zone microfluidic systems common to continuous-flow PCR, the spatial temperature resolution at the location of melting depends on its position over or between the heating zones, thereby complicating any correlation between temperature and fluorescence. Single-zone, steady-state gradient heating on the other hand, causes a constant rate of temperature change in the sample and allows for the precise mapping of the channel temperatures, which is conducive to high-resolution detection. This has been demonstrated both as an end-point technique (single cycle device) and as an *in situ* analysis during product amplification (30 cycle device).<sup>12</sup> Such was achieved by correlating fluorescent data from CCD images with a spatial temperature distribution determined from surface

<sup>a</sup>Department of Mechanical Engineering, University of Utah, Salt Lake City, UT 84112, USA. E-mail: gale@mech.utah.edu; Fax: (801) 585-9826; Tel: (801) 585-5944

<sup>b</sup>Department of Pathology, University of Utah, Salt Lake City, UT 84112, USA

temperature measurements under no-flow conditions. Thus, any significant flow-induced variation in the temperature profile of the device would create analytical error during a spatial DNA melting analysis and a reduction in the achievable efficiency and specificity of gradient PCR. Although flow-induced temperature fluctuations were not considered in this previous work, they should be minimized and/or characterized.

Hashimoto *et al.*<sup>2</sup> examined the effect of flow on the fluid temperature for a spiral microchannel within a polycarbonate (PC) substrate having a quadrant-heating configuration. To model the operation of their experimental device, a three-dimensional (3-D) model was developed. A single straight flow channel and surrounding material (substrate and insulating air gaps) were simulated, along with the appropriate heat sources. Adiabatic boundaries were assigned in the lateral directions to simulate symmetric boundaries associated with an infinite array of identical parallel channels (150  $\mu\text{m}$  deep  $\times$  50  $\mu\text{m}$  wide) spaced 150  $\mu\text{m}$  apart (center-to-center). The authors observed significant variation in the simulated fluid temperature over the range of examined volumetric flow rates (up to 9  $\mu\text{l min}^{-1}$ ). Similar thermal behavior was reported by Gui and Ren,<sup>14</sup> who developed a three-dimensional model of electro-osmotic flow (EOF) through a serpentine microchannel in a glass-PDMS substrate. A single U-shaped thermal cycle was considered, having the appropriate periodic thermal boundary conditions to simulate an infinite serpentine array. The bottom surface of the substrate was divided into three isothermal regions to cause multi-zone heating of the flowing fluid. An important finding of this work is the “temperature lag” that develops in the liquid as it both heats and cools, causing the heating fluid to be cooler and the cooling fluid to be warmer<sup>14</sup> than under no-flow conditions. While no correlation between this phenomenon and volumetric flow rate was discussed, this result is indicative of a local thermal sensitivity within such serpentine microfluidics.

This documented behavior can be attributed to the convection associated with the flowing fluid volume. Additionally, substrate axial conduction, which is typically neglected in most macroscale studies,<sup>15</sup> becomes a significant—if not dominant—factor in microfluidic thermal systems where axial temperature gradients can be on the order of  $10^3$   $^\circ\text{C m}^{-1}$ . Peterson,<sup>16</sup> in his study of the effect of axial conduction on the fluids in a microchannel counter-flow heat exchanger, indicated that increased heat exchange between the counter-flow microchannels reduces the temperature difference between the fluid and the surrounding solid.

This study examines the indirect heating of fluid within the single-cycle, two-pass channel geometry used for spatial DNA melting.<sup>12</sup> The effect of volume flow rate and temperature gradient are examined, as well as the material properties and channel spacing that control the thermal resistance between the straight counter-flow regions. It is assumed that the thermal mechanisms and trends associated with this two-pass design will be applicable to the operation of gradient PCR devices that use 60 or more counter-flow channel passes.<sup>10</sup> Since potential applications also include plug flow (multiple small sample volumes separated with an immiscible fluid), water, mineral oil, and air were examined for their effect on the thermal behavior of the system. By simulating steady-state device operation with each fluid independently, the resulting data was used to infer

the magnitude of the transient thermal effects that would occur within plug flow systems. Since recent spatial gradient PCR and DNA melting devices have demonstrated an optical resolution below 0.2  $^\circ\text{C pixel}^{-1}$ ,<sup>12</sup> this present work examines the range of device and operational parameters for which the flow-induced fluid temperature variation within any channel region does not exceed 0.2  $^\circ\text{C}$ .

## Methods

### Analytical

Some authors<sup>4,17</sup> discount the significance of flow-induced thermal effects in microfluidic systems based on a thermal mass comparison of the substrate and fluid. However, a simple evaluation of the interaction of the substrate temperature field with that of the fluid provides better insight into the expected response of the coupled system. For instance, consider the laminar flow of a single-phase fluid in a straight, circular, constant cross-section microtube embedded in a substrate with an imposed linear temperature gradient parallel to the tube. When considering the tube wall, the substrate temperature gradient is consistent with an isoflux boundary condition. If the flow is assumed to be fully developed, an expression for the fluid temperature at an axial location  $x$  in the tube as a function of radial position  $r$  in the tube is<sup>18</sup>

$$T(r) = T_s - \frac{2u_m}{\alpha} \frac{dT_m}{dx} \left( \frac{3r_0^2}{16} + \frac{r^4}{16r_0^2} - \frac{r^2}{4} \right) \quad (1)$$

where  $T_s$  is the temperature at the channel wall,  $u_m$  is the mean velocity,  $\alpha$  is the fluid thermal diffusivity,  $dT_m/dx$  is the mean axial temperature gradient of the fluid (equivalent to the axial temperature gradient of the tube wall), and  $r_0$  is the tube radius. Using eqn (1), the difference between the fluid mean temperature ( $T_m$ ) and the wall temperature is found to be

$$T_s - T_m = \frac{1}{6\pi} \frac{\dot{V}}{\alpha} \frac{dT_m}{dx} \quad (2)$$

where  $\dot{V}$  is the volumetric flow rate. The heat rate per unit length  $q'$  is expressed as

$$q' = hP(T_s - T_m) \quad (3)$$

where  $P$  is the tube perimeter and  $h$  is the heat transfer coefficient. For the prescribed conditions, the Nusselt number,  $\text{Nu}$ , is constant, and is defined as

$$\text{Nu} = \frac{hD}{k} \quad (4)$$

where  $D$  is the tube diameter and  $k$  is the fluid thermal conductivity. Combining eqn (2)–(4) yields

$$q'_{\text{wall}} = \frac{1}{8} \text{Nu} \dot{V} \rho c_p \frac{dT_m}{dx} \quad (5)$$

where  $\rho$  is the fluid density and  $c_p$  is the fluid specific heat at constant pressure. Eqn (1) indicates that the maximum temperature difference between the fluid and the wall is proportional to

the mean velocity and the imposed axial temperature gradient in the substrate and is inversely proportional to the thermal diffusivity. Eqn (2) indicates that the difference in the fluid mean temperature and the wall temperature is proportional to  $\dot{V}$  and is also inversely proportional to  $\alpha$ . Additionally, eqn (5) indicates that, for constant properties, the convection heat rate will be controlled by  $\dot{V}$  and the imposed axial temperature gradient  $dT/dx$ , independent of the channel diameter. The total fluid temperature change at a particular location caused by its flow is the sum of the temperature difference between the fluid and wall (see eqn (2)) and the change in the wall temperature resulting from the inter-channel conduction. As indicated above, this coupled process will be dependent on  $\dot{V}$ , fluid properties, and the transverse thermal resistance in the substrate, which is a function of channel separation distance and substrate thermal conductivity. It should be noted that this temperature change is related to the volume flow rate, *not* the mean velocity, of the fluid. Thus, the specific cross-sectional area of the microchannel is irrelevant, which allows for simplification of the computational model, and expansion of the applicability of this present study.

## Experimental

### Device fabrication

Glass microchips were manufactured according to a previously reported design<sup>12</sup> and protocol.<sup>11</sup> Three channels were fabricated on the device, for independent testing. Each channel consists of a single pair of counter-flow segments, 1 cm in length, having a center-to-center spacing ( $L$ ) of 1 mm, 3 mm, or 5 mm. All channels were etched to a depth of 100  $\mu\text{m}$  with a width of 600  $\mu\text{m}$ . During testing, the device was placed in a heating fixture with the channel of interest oriented such that the fluid enters along an isotherm, is heated, cooled, and then exhausted from the channel along the initial isotherm.

### Temperature measurement

A steady-state temperature gradient was created within the glass substrate by two strip heaters (5 mm  $\times$  75 mm) attached to the underside of the glass microchip on the longitudinal edges, as previously detailed.<sup>11</sup> An infrared (IR) camera (Thermacam PM390, Inframetrics Inc., MA, USA) was used to measure the spatial temperature distribution on the top surface of the fabricated device. The spectral window of the IR camera (3.4–5  $\mu\text{m}$ ) was such that the camera could detect both emitted and transmitted radiation from the microchip, elevating and distorting the temperature reading of the glass surface. Thus, test devices were spray-painted black (top surface only) to minimize transmitted IR and to give the surface a known emissivity (0.95). With a painted device positioned in the heating apparatus, a working voltage of 5.7 V was applied to the heater pair beneath one edge of the chip, and a voltage of 2.5 V was applied to the heater pair beneath the base of the cooling fins under the opposite edge of the substrate. These voltages were designed to produce edge temperatures of approximately 100  $^{\circ}\text{C}$  and 50  $^{\circ}\text{C}$ , respectively. The camera was positioned above the heated device, with the field of view centered over the channel under investigation. Commercial microfluidic connectors and tubing (Upchurch Scientific, WA, USA) were used to interface a micro-

volume syringe (Hamilton Company, NV, USA) and syringe pump (#KDS120, KD Scientific, MA, USA) to the drilled inlet port of the channel. Purified water was pumped through the microchannel at volumetric flow rates up to 3  $\text{ml h}^{-1}$  (50  $\mu\text{l min}^{-1}$ ). At each  $\dot{V}$ , the chip was imaged with the thermal camera after 2 min of continuous flow. For each set of experiments, the device was tested and imaged at least three times at all target volumetric flow rates to ensure acceptable accuracy and repeatability of the temperature measurements.

The thermal images were analysed using TherMonitor<sup>TM</sup>, the camera's companion software (Thermoteknix Systems Ltd, Cambridge, UK). The flow-induced distortions of the temperature gradient were quantified by examining the normalized temperature distribution [ $\theta_A(y)$ ] along line A and the temperature difference [ $\Delta T_{BC}(x) = T_B - T_C$ ] between lines B & C (lines A, B & C are indicated in Fig. 1, where line C is along the channel section where fluid flow is toward higher temperatures, and line B is where fluid flow is toward cooler temperatures). To normalize the data for  $\theta_A$ , the temperature ( $^{\circ}\text{C}$ ) at each point along line A was divided by the temperature ( $^{\circ}\text{C}$ ) at  $y = 0$  [ $\theta_A(y) = T_A(y)/T_A(0)$ ]. Temperatures from at least 130 points along each line were used. The data from the three channel spacings ( $L = 1, 3, \text{ and } 5 \text{ mm}$ ) and from three volumetric flow rates ( $\dot{V} = 1, 2, \text{ and } 3 \text{ ml h}^{-1}$ ) were used to validate the numerical model.

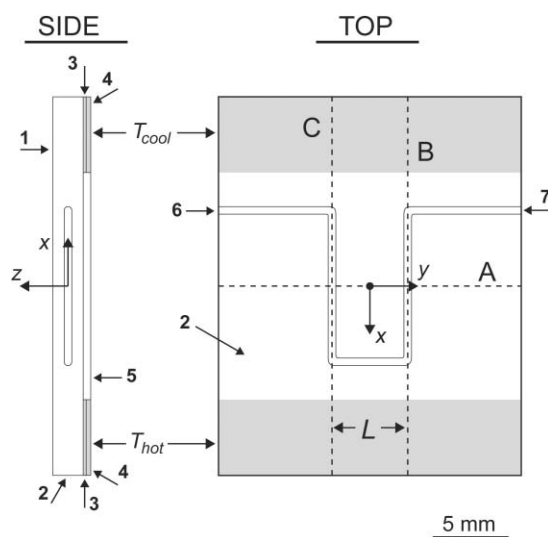


**Fig. 1** A side and top view of the SolidWorks/COSMOSFloWorks model. Dimensions are to scale, as shown. Dashed lines A, B & C represent planes through which temperature data were collected. A is collinear with the  $y$ -axis, B indicates the region of the channel where the fluid is cooling, and C identifies the channel section where fluid heating occurs. The numbered features in this diagram indicate: 1, top surface of the model; 2, substrate; 3, thermal interface pads; 4, aluminium strips; 5, insulator; 6, channel inlet; 7, channel outlet.  $T_{cool}$  and  $T_{hot}$  refer to the temperatures set as boundary conditions.

The measurement uncertainty of the IR camera was determined using a thermocouple and heated copper block. The polished copper block was painted in the same way as the glass test article. Using a hot plate, the copper block was heated until steady-state thermal conditions were achieved. Temperature data from the IR camera were examined along an arbitrary line crossing the heated block, consisting of more

than 180 pixels. A 4th order polynomial provided the best fit to this resulting temperature distribution, and the variations between the recorded temperatures and the fit curve were used to compute a measurement uncertainty ( $\pm 0.116\text{ }^\circ\text{C}$  or  $\pm 0.236\%$ ).

### Numerical method

A computational model with a two-pass channel design similar to the experimental device was developed using COSMOSFloWorks™, the CFD (computational fluid dynamics) companion to the CAD (computer-assisted design) software SolidWorks™ (SolidWorks Corporation, Concord, MA, USA), to examine the thermal behavior of the substrate and fluid. The computational analysis provides the solution of the momentum and energy equations in the fluid and the energy equation in the solid for the temperature field. Idealizations included steady-state behavior, fully-developed flow at the channel inlet, convection boundary conditions on the top ( $x$ - $y$  face) and two side surfaces ( $x$ - $z$  faces only), and no internal generation. COSMOSFloWorks uses the finite volume approach to the solution of conjugate heat transfer problems after discretizing the CAD model into three types of cuboid (rectangular prism) cells: solid cells, fluid cells, and partial cells (which encompass all solid/fluid interfaces). Thermal performance of the microfluidic device was simulated for the three  $L$ -values and four volumetric flow rates ( $\dot{V} = 0, 1, 2, \& 3\text{ ml hr}^{-1}$ ). Measured surface temperature data were used to validate the model, after which non-tested device configurations were simulated. The computational model, shown in Fig. 1, includes a serpentine channel passing through the mid-plane of the substrate ( $22\text{ mm} \times 25\text{ mm} \times 2\text{ mm}$ ) with the same centerline geometry as one of the channels in the experimental device. Adhesive thermal pads ( $5\text{ mm} \times 22\text{ mm} \times 0.2\text{ mm}$ ,  $k = 0.9\text{ W m}^{-1}\text{ K}^{-1}$ ) are located in parallel beneath the long edges of the substrate with their long axis in the  $y$ -direction. Aluminium strips ( $5\text{ mm} \times 22\text{ mm} \times 0.3\text{ mm}$ ) contact the thermal interface pads. The region on the bottom of the microchip between the heating and cooling elements ( $15\text{ mm} \times 22\text{ mm} \times 0.5\text{ mm}$ ) was modeled as a perfect insulator. Based on the analytical work just presented, it was not necessary that the simulated microfluidic channel have a cross-section identical to the high aspect ratio etched channel. Thus, for computational simplicity, a circular cross-section was used, having a uniform diameter of  $500\text{ }\mu\text{m}$ . The flowing fluid was modeled as water. The channel inlet was assigned a volumetric flow rate with a fully developed laminar velocity profile, and the outlet was designated as an atmospheric pressure boundary. The channel segments at the inlet and outlet were designed to lay along an isotherm under no-flow conditions. The fluid temperatures at the inlet and outlet boundaries were assigned the temperature of the corresponding isotherm. The convective exterior surfaces of the glass were assigned a heat transfer coefficient ( $h$ ) of  $10\text{ W m}^{-2}\text{ K}^{-1}$  and a nominal ambient temperature ( $T_\infty$ ) of  $20.05\text{ }^\circ\text{C}$  was assumed. The two aluminium strips were also assigned temperatures, such that the resulting maximum and minimum surface temperatures (for  $\dot{V} = 0\text{ ml hr}^{-1}$ ) would closely match those of the experimental device under similar conditions. This temperature matching process required iteration on the set temperatures at the heater surfaces. The appropriate level of mesh refinement was also determined iteratively. The desired refinement was defined as

the lowest mesh setting for which further refinement would affect the numerical solution by less than  $0.02\%$ . In addition to this general setting, the minimum cell density within the simulated microchannel was assigned such that the meshed channel would be at least seven elements across. These settings produced approximately 19 000 fluid cells, 67 000 solid cells, and 48 000 partial cells. A series of simulations were performed, in which the parameters of interest were independently modulated.

## Results and discussion

### Validation of the model

By heating the device as previously explained,<sup>12</sup> a no-flow steady-state temperature gradient was reached in approximately 10 minutes. The temperature on the surface of the device ranged from approximately  $100\text{ }^\circ\text{C}$  above the high-voltage heater to approximately  $50\text{ }^\circ\text{C}$  above the low-voltage heater. Since the channel was limited to the middle  $1\text{ cm}$  of the device, the fluid only experienced a temperature range of approximately  $58\text{--}82\text{ }^\circ\text{C}$ . Once the temperature gradient stabilized, water flow was established within a selected microchannel at the desired volumetric flow rate. Thermal images from the IR camera revealed measurable surface temperature variation. Isotherms that were parallel to the heaters with no flow became distorted with flow, with the greatest displacement being directly over the counter-flow sections. This effect is clearly shown in Fig. 2 for a single isotherm.

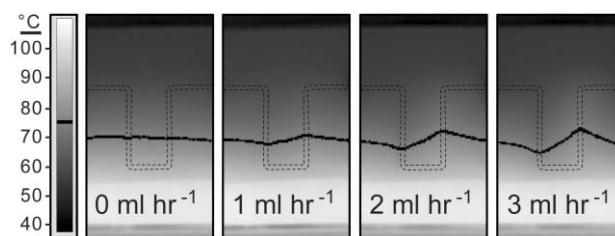


**Fig. 2** Infrared images show the effect of volumetric flow rate on an isotherm across a counter-flow channel having  $L = 5\text{ mm}$ . Fluid flow is from left to right. The dark bar in the scale shows the temperature of the isotherm in the subfigures. A dotted outline of the microchannel is overlaid on these thermal images to indicate its approximate location.

Simulations were performed with the two-pass numerical model using the same parameters ( $\dot{V}$ ,  $L$ , etc.) as the experimental device. Temperature data from the model were found to agree with the experimental data both in trend and in absolute value for all three channel spacings ( $1\text{ mm}$ ,  $3\text{ mm}$ , and  $5\text{ mm}$ ) and all three values of  $\dot{V}$  ( $1, 2, \& 3\text{ ml hr}^{-1}$ ). Experimental and numerical data for several of these cases are shown in Fig. 3.  $\Delta T_{BC}$  for several volumetric flow rates through a channel with  $L = 1\text{ mm}$  is shown in Fig. 3a. For no-flow conditions, the experimental  $\Delta T_{BC} \neq 0$  due to longitudinal ( $y$ -direction) inconsistencies in  $dT/dx$ , caused by imperfect heating on the two edges and irregularities in device cooling by natural convection. To remove this effect, the no-flow  $\Delta T_{BC}$  was subtracted from  $\Delta T_{BC}$  for the non-zero volumetric flow rates. The average variation between the numerical and experimental  $\Delta T_{BC}$  values for all non-zero  $\dot{V}$  was  $\pm 0.104\text{ }^\circ\text{C}$ , which is less than the measurement uncertainty of the system. Normalized surface temperatures [ $\theta_A(y)$ ] along

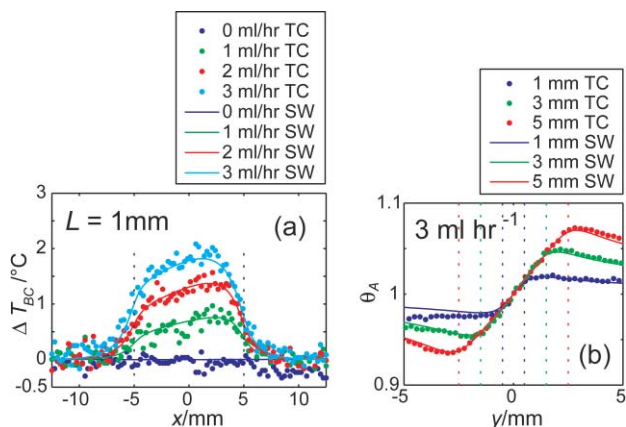


**Fig. 3** A comparison of the experimental and numerical data is shown. Plot (a) gives the surface temperature difference between lines B & C ( $\Delta T_{BC} = T_B - T_C$ ) for four volumetric flow rates in a glass device having  $L = 1$  mm. Vertical dashed lines in (a) indicate the position of the microfluidic channel. Normalized surface temperature along line A ( $\theta_A$ ) for the three channel spacings with  $\dot{V} = 3$  ml h<sup>-1</sup> is shown in (b). Dashed vertical lines show the relative centerline position of the three sets of counter-flow channels. The legend indicates the center-to-center channel spacing ( $L = 1, 3$ , or  $5$  mm) and the data source (TC-ThermaCam, or SW-SolidWorks/FloWorks).

line A from the experiment and simulations are compared in Fig. 3b for all three  $L$ -values for  $\dot{V} = 3$  ml h<sup>-1</sup>. The average variation between the experimental and numerical data in the range  $-5 \leq y < 5$  mm on line A was  $\pm 0.336\%$  for all non-zero  $\dot{V}$ . While this average variation is larger than the measurement uncertainty of the experimental system, the majority of this disagreement occurs away from the channel pair, which may be attributed to a numerical misrepresentation of the natural convection occurring on the surfaces of the experimental device (e.g. Fig. 3b, '1 mm TC'). By considering only the data from the region that closely surrounds the counter-flow channel sections, the experimental and numerical data agree to within the measurement uncertainty. Thus, it is concluded that the model and experiment yield the same thermal results, and that further simulations of additional device configurations would accurately predict thermal behavior.

## Parametric results

### Comparison of surface and fluid temperatures

While the experimental measurements only provide temperature data at the surface of the device, the numerical analysis gives information at every element in the model, which allows for an examination of the thermal behavior within the substrate and channels. Temperature data along lines B ( $T_B$ ) and C ( $T_C$ ) (from Fig. 1) at the top surface and the mid-plane of the substrate ( $z = 0$ ), illustrate the greater thermal variation at the device mid-plane, as shown in Fig. 4. As expected for  $\dot{V} = 0$  ml h<sup>-1</sup>, there is no apparent difference between the heating (line C) and cooling (line B) channel temperatures, and the surface temperature is less than that at the mid-plane. These temperature differences are greater as the substrate temperature increases, due to the increase in heat transfer to the top surface. The slight non-linearity of the temperature gradient within the fluid

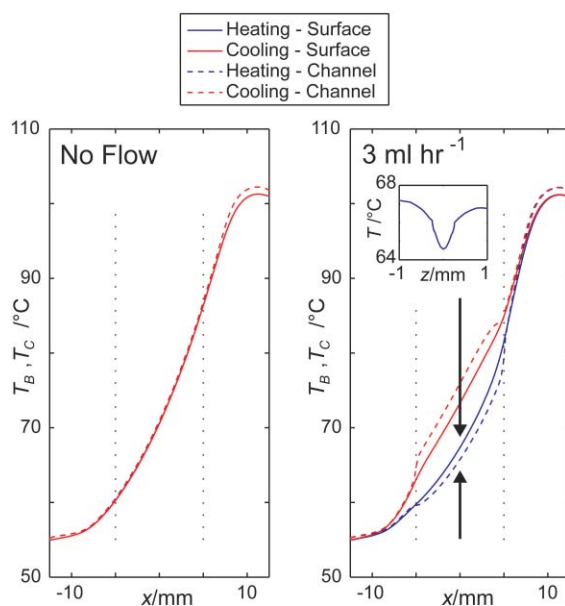


**Fig. 4** A comparison between temperatures along lines B & C ( $T_B$  and  $T_C$ , respectively) at the top surface ( $z = 1$  mm) and mid-plane ( $z = 0$  mm) of a glass device with  $L = 3$  mm. The vertical dotted lines indicate the position of the microchannel. Natural convection from the top surface was included in the model, and the set temperatures of the aluminium strips were  $110$  °C and  $50$  °C. The inset shows a plot of the temperature distribution in the  $z$ -direction at  $x = 0$  and  $y = -1.5$  mm (line C).

is caused by natural convection effects at the top surface. Natural convection produces nominal heat loss at the  $x$ - $z$  end surfaces. These same general effects are also evident for the  $\dot{V} = 3$  ml h<sup>-1</sup> case. For this volumetric flow rate, the maximum temperature difference between the two fluids at a cross section is on the order of  $10$  °C, resulting in significant heat exchange between the two fluids. Note that the temperature difference between the surface and channel is larger for the cooling channel than for the heating channel, since immediately above the heating channel, heat is transferred from the substrate to the heating fluid and the surface (see the inset in Fig. 4), while above the cooling channel, heat is transferred only from the cooling fluid to the surface. A qualitative comparison with numerical results by Peterson,<sup>16</sup> shows significant agreement in the thermal behavior of the fluid. A comparison of  $\theta_A$  data at the surface and mid-plane is shown in Fig. 5. The transverse temperature gradient within the solid between the channels is linear and independent of channel spacing, but not  $\dot{V}$ . This linearity indicates that the diffusion process is highly one-dimensional and driven by the fluid temperature difference between the two channels. As expected, significant temperature change occurs within the fluid and in the closely surrounding substrate. These results support the previous explanation of the thermal mechanisms involved. The temperature distribution within each channel is similar to that given in eqn (1). Also as expected, the temperature difference between the wall and the fluid increases with volumetric flow rate giving rise to increased diffusion.

### Counter-flow channel spacing

For further examination of thermal effects in the microfluidic device, the B–C temperature difference at  $x = 0$  [ $\Delta T_{BC}(A)$ ] will be

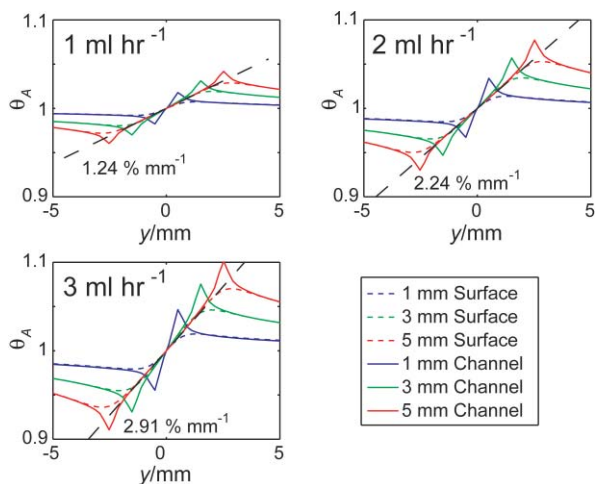


**Fig. 5**  $\theta_A$  at the surface and at the depth of the embedded channel. Data for  $L = 1, 3, \& 5$  mm are shown for  $\dot{V} = 1, 2, \& 3$  ml h<sup>-1</sup>. The diagonal line in each sub-figure is fit to the overlapping linear regions of the six curves.

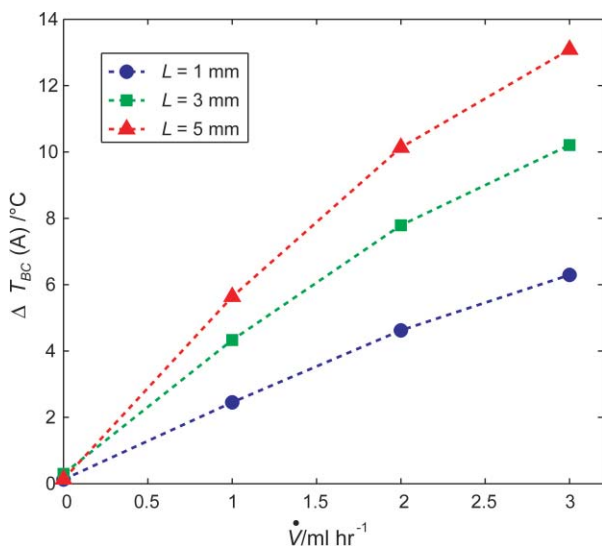


**Fig. 6** Effect of  $\dot{V}$  on  $\Delta T_{BC}(A)$  for a glass model.

used as the representative measure of the maximum temperature difference between counter-flow channel regions.  $\Delta T_{BC}(A)$  is shown as a function of  $\dot{V}$  in Fig. 6. Glass was used as the substrate material and natural convection at the surface of the model was included. For  $\dot{V} \leq 2$  ml h<sup>-1</sup>,  $\Delta T_{BC}(A)$  is proportional to  $\dot{V}$ . The effect of  $L$  on  $\Delta T_{BC}(A)$  is also nearly linear, as expected for one-dimensional diffusion. Increasing  $L$  increases thermal resistance, requiring a larger temperature difference for the inter-channel heat transfer.

### Fluid properties

Water, mineral oil, and air are commonly used in microfluidic PCR and lab-on-a-chip devices for droplet-based applications. In such systems, multiple aqueous droplets separated by air, oil, or another immiscible fluid are passed through heated microfluidic channels. Steady-state simulations using these three fluids produce data (not shown) indicating that an equal  $\dot{V}$  of

mineral oil causes  $\Delta T_{BC}(A)$  to increase approximately 12% over that for water.  $\Delta T_{BC}(A)$  is near zero for air flow with  $\dot{V} \leq 3$  ml h<sup>-1</sup>. These results are expected due to the relative magnitude of  $\alpha$  for the three fluids and its effect on the convection heat transfer within the channels (see eqn (1)). Since the respective fluids cause a different amount of temperature change within the fluid, it can be concluded that fluid combinations, such as with plug flow, would cause transient fluctuation of the temperature in the fluid and substrate. This unsteady behavior is predicted to be more pronounced when aqueous sample plugs are separated by air than by oil.

### Effect of substrate temperature gradient

The axial temperature gradient ( $dT/dx$ ) in the substrate was varied by assigning different pairs of temperatures to the aluminium strips beneath the outer edges of the substrate. To linearize the gradient in the region of the microchannel, surface convection was excluded from the model during the examination of the substrate temperature gradient's influence on the thermal flow effects. Temperature pairs of (100, 70 °C), (110, 50 °C), and (120, 30 °C) were simulated, and a fit of the resulting data approximated linear temperature gradients of 1.7 °C mm<sup>-1</sup>, 3.5 °C mm<sup>-1</sup>, and 5.2 °C mm<sup>-1</sup> along the microchannel, respectively. A two-pass glass device was modeled, with  $L = 1$  mm. The fluid was simulated as water, with  $\dot{V} = 2$  ml h<sup>-1</sup>.  $\Delta T_{BC}(A)$  associated with each gradient was found to be 3.0, 6.0, and 9.1 °C. This linear relationship between the  $dT/dx$  and  $\Delta T_{BC}(A)$  is analogous to the relationship between  $dT_m/dx$  and  $q'_{wall}$  shown in eqn (5).

### Substrate material

The effect of substrate material on the thermal behavior of the microchannel fluid was also investigated. Common substrate materials for microfluidic devices include polymers ( $k \approx 0.1$  W m<sup>-1</sup> K<sup>-1</sup>) and silicon ( $k \approx 100$  W m<sup>-1</sup> K<sup>-1</sup>). The effect of volumetric flow rate on  $\Delta T_{BC}(A)$  for substrate thermal conductivities of 10<sup>-1</sup>, 10<sup>0</sup>, 10<sup>1</sup>, and 10<sup>2</sup> is shown in Fig. 7. The fluid was modeled as water, with  $L = 1$  mm, and  $dT/dx = 3.5$  °C mm<sup>-1</sup>.  $\Delta T_A$  increases with a decrease in  $k$ . For a fixed  $\dot{V}$  and  $dT/dx$ , convection is nearly constant in the adjacent channels (see eqn (5)). Thus, the increasing inter-channel thermal resistance (decreasing  $k$  with  $L$  constant) produces a larger  $\Delta T_{BC}(A)$ . As demonstrated previously,  $\Delta T_{BC}(A)$  is nearly proportional to  $\dot{V}$ . In most thermal microfluidic applications, low  $\Delta T_{BC}(A)$  is desired, suggesting a material with high  $k$  should be selected. However, energy costs for maintaining the desired axial temperature gradient in the substrate would also increase for the high  $k$  material. An estimate of the minimum temperature offset is also included in Fig. 7. This analytical temperature offset ( $\Delta T_{anal}$ ), defined similarly to  $\Delta T_{BC}(A)$ , is equivalent to twice the maximum fluid temperature change in one of the microchannels

$$\Delta T_{anal} = 2 | T_{fluid}(r = 0) - T_{wall} | \quad (8)$$

from eqn (1). As expected from eqn (5),  $\Delta T_{anal}$  is linearly related to  $\dot{V}$ . This estimate is based on an assumption of infinite substrate  $k$ , meaning that the only inter-channel temperature change occurs within the counter-flowing fluids. Eqn (8) includes the constraints associated with eqn (1), primarily the assumption

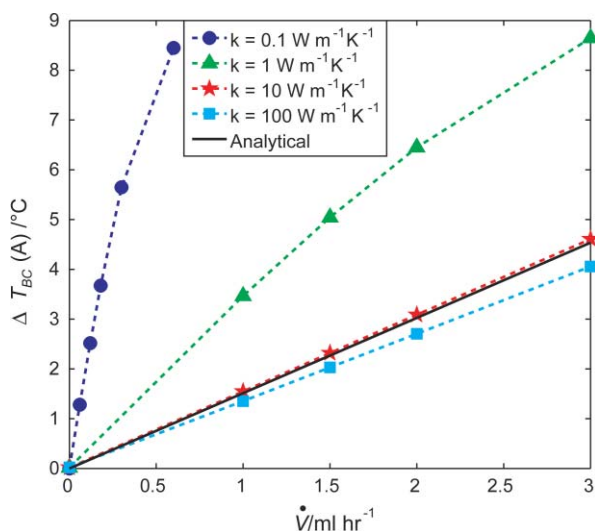


**Fig. 7**  $\Delta T_{BC}(A)$  as a function of  $\dot{V}$  is shown for four substrate thermal conductivities. An insulated model was used, with an effective axial temperature gradient of  $3.5\text{ }^{\circ}\text{C mm}^{-1}$ . The solid line indicates  $\Delta T_{anal}$  from eqn (8).

of an isoflux boundary condition and fully-developed flow in a straight circular tube. These assumptions, and the error that results, are the reasons that the estimate does not appear to be a limiting case in Fig. 7. Since the inter-channel substrate diffusion is three-dimensional, an isoflux boundary condition only approximates the actual boundary condition on the channel walls. The numerical results presented in this work indicate that there can be significant temperature change in the channel wall temperatures. The data in Fig. 6 and 7 indicate that the temperature shift is highly dependent on channel spacing and substrate thermal conductivity. In more general terms, the temperature shift is highly dependent on the substrate thermal resistance.

### Operational conditions

For microfluidic applications such as gradient DNA melting analysis and gradient PCR, it is desired to have an operational range over which the fluid temperature is independent of its flow characteristics. A flow-induced temperature variation of less than  $0.2\text{ }^{\circ}\text{C}$  approaches the limit of resolution previously reported.<sup>12</sup> Since  $\Delta T_{BC}(A)$  is the cumulative variation associated with both counter-flow channel sections, the maximum allowable  $\Delta T_{BC}(A)$  is designated as  $0.4\text{ }^{\circ}\text{C}$ . For aqueous fluids, eqn (1), suggests that  $\dot{V} \leq 4.4\text{ }\mu\text{l min}^{-1}$  ( $0.263\text{ ml h}^{-1}$ ) with  $dT/dx = 3.5\text{ }^{\circ}\text{C mm}^{-1}$  would adequately satisfy this condition, regardless of the substrate material or counter-flow nature of the channel design. However, a much lower  $\dot{V}$  can actually cause  $\Delta T_{BC}(A)$  to exceed this imposed limit, since the net fluid temperature variation is the combination of the temperature difference between the fluid and the channel wall (see eqn (1)) and the temperature change in the channel wall itself. For example, water flowing through a polymer substrate with  $L = 1\text{ mm}$  and  $k = 0.1\text{ W m}^{-1}\text{ K}^{-1}$  achieves the imposed  $0.4\text{ }^{\circ}\text{C}$  temperature limit when  $\dot{V} = 0.32\text{ }\mu\text{l min}^{-1}$  ( $0.02\text{ ml h}^{-1}$ ), more than an order of magnitude lower than predicted by eqn (8). Glass would permit an approximately five-fold increase in  $\dot{V}$  over many polymer

substrates. By using glass microfluidics with  $L \leq 1\text{ mm}$ ,  $dT/dx \leq 3.5\text{ }^{\circ}\text{C mm}^{-1}$ , and  $\dot{V} \leq 2\text{ }\mu\text{l min}^{-1}$  ( $0.12\text{ ml h}^{-1}$ ),  $\Delta T_{BC}(A)$  will not exceed  $0.4\text{ }^{\circ}\text{C}$ . Under such conditions, the thermal map of the microfluidic channel would not noticeably vary during either continuous, or plug flow. A subsequent decrease in  $L$  would provide an effectively linear increase in the allowable  $\dot{V}$ . While halving the imposed  $dT/dx$  would double the limiting  $\dot{V}$ ,  $3.5\text{ }^{\circ}\text{C mm}^{-1}$  conveniently generates the ideal temperature distribution ( $60\text{--}95\text{ }^{\circ}\text{C}$ ) for PCR applications<sup>12</sup> over only  $1\text{ cm}$  of axial channel length.

### Conclusion

The flow-induced thermal effects of microscale fluid flow through a temperature gradient parallel to counter-flow channels have been examined. Local thermal effects can have a significant influence on the temperatures experienced by the traveling fluid and should not be neglected without consideration. The results of this present study indicate that a counter-flow channel configuration can reduce flow-induced temperature changes, and that the extent of this reduction is a function of the heat transfer between counter-flow regions. While the temperature difference between the fluid and channel wall is largely governed by volumetric flow rate and fluid properties, the temperature shift experienced by the channel wall is significantly affected by the inter-channel substrate thermal resistance. The substrate thermal conductivity and the channel separation distance dictate this resistance. Reduced spacing and a higher thermal conductivity lowers the temperature shift in the channel walls, thus minimizing the overall temperature change experienced by the fluid. However, since such substrates also require greater energy consumption to maintain the imposed axial temperature gradient, care should be taken in material selection. In addition, the transient thermal effects associated with multi-phase or multi-component fluid samples should be considered, especially in operational regimes where the flow-induced thermal variations may be significant. A transient analysis of such flow would be a valuable continuation of this present study. Further work could also be directed toward the expansion of the two-pass geometry, by investigating the thermal behavior of serpentine arrays of multiple counter-flow sections. Since this work focused on single-material substrates, thermal flow effects within common multi-material microfluidic devices such as glass–silicon, glass–PDMS, and Xurographic laminates would also be a valuable direction of further study.

This work has led to the thermal characterization of a two-pass serpentine microfluidic geometry under the influence of steady-state flow and temperature gradient heating. While the relevance of the specific thermal fluctuations obtained in this study may be limited to comparable systems, the thermal trends that have been characterized are of general importance. For any microfluidic application that requires an accurate thermal mapping of the fluid and substrate, the trends discussed in this work should be considered during device design and operation.

### Acknowledgements

Authors credit funding by the State of Utah Center of Excellence program and the University of Utah College of Engineering NSF IGERT Program.

---

## References

- 1 M. U. Kopp, A. J. de Mello and A. Manz, *Science*, 1998, **280**, 1046–1048.
- 2 M. Hashimoto, P. C. Chen, M. W. Mitchell, D. E. Nikitopoulos, S. A. Soper and M. C. Murphy, *Lab Chip*, 2004, **4**, 638–645.
- 3 P. J. Obeid, T. K. Christopoulos, H. J. Crabtree and C. J. Backhouse, *Anal. Chem.*, 2003, **75**, 288–295.
- 4 S. F. Li, D. Y. Fozdar, M. F. Ali, H. Li, D. B. Shao, D. M. Vykoukal, J. Vykoukal, P. N. Floriano, M. Olsen, J. T. McDevitt, P. R. C. Gascoyne and S. C. Chen, *J. Microelectromech. Syst.*, 2006, **15**, 223–236.
- 5 I. Schneegass, R. Brautigam and J. M. Kohler, *Lab Chip*, 2001, **1**, 42–49.
- 6 J. A. Kim, J. Y. Lee, S. Seong, S. H. Cha, S. H. Lee, J. J. Kim and T. H. Park, *Biochem. Eng. J.*, 2006, **29**, 91–97.
- 7 T. Nakayama, Y. Kurosawa, S. Furui, K. Kerman, M. Kobayashi, S. R. Rao, Y. Yonezawa, K. Nakano, A. Hino, S. Yamamura, Y. Takamura and E. Tamiya, *Anal. Bioanal. Chem.*, 2006, **386**, 1327–1333.
- 8 H. Wang, J. F. Chen, L. Zhu, H. Shadpour, M. L. Hupert and S. A. Soper, *Anal. Chem.*, 2006, **78**, 6223–6231.
- 9 H. B. Mao, M. A. Holden, M. You and P. S. Cremer, *Anal. Chem.*, 2002, **74**, 5071–5075.
- 10 N. Crews, C. Wittwer and B. Gale, *Proc. SPIE-Int. Soc. Opt. Eng.*, 2007, **6465**, 646504.
- 11 N. Crews, C. Wittwer and B. Gale, *Biomed. Microdevices*, 2008, **10**, 187–195.
- 12 N. Crews, C. T. Wittwer, R. Palais and B. Gale, *Lab Chip*, 2008, **8**(6), 919–924.
- 13 K. M. Ririe, R. P. Rasmussen and C. T. Wittwer, *Anal. Biochem.*, 1997, **245**, 154–160.
- 14 L. Gui and C. L. Ren, *Anal. Chem.*, 2006, **78**, 6215–6222.
- 15 F. Incropera, D. Dewitt, T. Bergman and A. Lavine, *Fundamentals of Heat and Mass Transfer*, John Wiley and Sons, Hoboken, 6th edn, 2007, pp. 669–705.
- 16 R. B. Peterson, *Nanoscale Microscale Thermophys. Eng.*, 1999, **3**, 17–30.
- 17 Q. Zhang, W. Wang, H. Zhang and Y. Wang, *Sens. Actuators, B*, 2002, **82**, 75–81.
- 18 W. M. Kays and M. E. Crawford, *Convective Heat and Mass Transfer*, McGraw-Hill, New York, 3 edn, 1993.